Article

Li$_4$Ti$_5$O$_{12}$ Coated by Biomass-Derived Carbon Quantum Dots as Anode Material with Enhanced Electrochemical Performance for Lithium-Ion Batteries

Marcin Krajewski [1,*], Chun-Hao Chen [2], Zhi-Ting Huang [3] and Jeng-Yu Lin [3,*]

1 Institute of Fundamental Technological Research, Polish Academy of Sciences, Pawińskiego 5B, 02-106 Warsaw, Poland

2 Department of Chemical Engineering and Biotechnology, Tatung University, No. 40, Sec. 3, Chungshan N. Rd., Taipei City 10452, Taiwan

3 Department of Chemical and Materials Engineering, Tunghai University, No. 181, Sec. 3, Taichung Port Rd., Taichung City 40704, Taiwan

* Correspondence: mkraj@ippt.pan.pl (M.K.); jylin@thu.edu.tw (J.-Y.L.)

Abstract: Li$_4$Ti$_5$O$_{12}$ (LTO) is a promising anode material for lithium-ion batteries (LIBs) due to its stable reversibility, high-rate cyclability, and high operational potential. On the other hand, it suffers from poor electronic conductivity and low capacitance. To overcome these disadvantages, modification of the LTO surface is frequently undertaken. Considering this idea, the production of a biomass-derived carbon-coated LTO material (LTO/C) and its application as an anode in LIBs is described in this work. The carbon precursor was obtained from commercial carrot juice, which was degraded using microwaves. According to the UV studies, the carbon precursor revealed similar properties to carbon quantum dots. Then, it was deposited on LTO synthetized through a sol-gel method. The LTO/C electrode exhibited a high specific capacity of 211 mAhg^{-1} at 0.1 C. Capacity retention equal to 53% of the initial value was found for the charge–discharge rate increase from 0.1 C to 20 C. The excellent electrochemical performance of LTO/C was caused by the carbon coating, which provided (i) short diffusion pathways for the Li$^+$ ions into the LTO structure and (ii) enhanced electronic conductivity. The obtained results indicated that biomass-derived carbon quantum dot-coated LTO can be considered as a promising anode for LIBs.

Keywords: anode material; biomass-derived carbon; carbon coating; carbon quantum dot; lithium-ion battery

1. Introduction

In the era of electromobility, rechargeable energy storage devices play a very important role. Thus far, lithium-ion batteries (LIBs) have been achieved success in the market and have become the most widely used rechargeable energy storage systems due to their excellent rechargeability, suitable power density, and outstanding energy density, as well as long cycling life [1,2]. LIBs are typically composed of three primary elements, i.e., a positive electrode (cathode), a negative electrode (anode), and an electrolyte. To improve the electrochemical performance of this type of batteries, investigations on each of these elements are important. However, the search for new or the optimization of already known anode materials that would constitute a good alternative for the commercial graphite electrodes is a crucial issue [3,4]. In general, anode materials with long life, thermodynamic stability, enhanced safety, excellent electrochemical performance, and high-rate cyclability are highly appreciated. Among these, a spinel lithium titanium oxide (Li$_4$Ti$_5$O$_{12}$; LTO) is considered as one of the most promising candidates to satisfy the features mentioned above [4–6].

LTO anode material is known for its zero-strain nature, i.e., no volume changes during the lithiation–delithiation processes. Besides that, an LTO electrode operates at a potential

above 1.55 V vs. Li$^+$/Li. This means that electrolyte decomposition and consecutive formation of a solid-electrolyte interphase (SEI) layer on the LTO surface are avoided. These features of the material influence its enhanced safety, high voltage platform, perfect cycling performance, and long-life [5,6]. On the other hand, LTO possesses some serious drawbacks. For instance, its theoretical capacity (175 mAh g^{-1}) is lower than graphite (372 mAh g^{-1}). LTO electrodes also suffer from a poor intrinsic electronic conductivity (10^{-13} S cm^{-1}) and a low lithium-ion diffusion coefficient (10^{-9}–10^{-13} cm^2 s^{-1}) [6–8]. To minimize the impact of LTO's disadvantages, many LTO modifications have been already postulated. Among them, four strategies are very common, namely: (i) reduction of LTO particle size to nanoscale [9–11], (ii) metallic and non-metallic doping of LTO [12–16], (iii) selection of a proper titanium precursor [17], and (iv) surface modification [18–23].

Thus far, the surface modification of LTO electrode material has received particular attention. This strategy is usually realized by the deposition of various coatings on the LTO surface. Among many successfully deposited coatings, carbon coatings are one of the most frequently studied because they aim to improve the interphase chemistry, electrical conductivity, and mechanical integration [3,6]. In addition, the presence of carbon coating provides fast lithium-ion diffusion. Carbon coatings are commonly obtained by mixing the various carbon precursors with LTO or its precursors and their subsequent annealing at high temperatures in an inert or reducing atmosphere [8,18–20,24–26]. Recently, a new trend to transform biomass into useful biocarbons has been appeared in the scientific community. Such a strategy has been successfully used by K.Q. Lia et al. [27] to obtain a carbon coating from phoenix tree leaves for LTO material. Their carbon-coated LTO electrode has revealed a great electrochemical performance, i.e., a reversible capacity of 201 mAh g^{-1} after 500 cycles measured at charge/discharge current density of 175 mA g^{-1} (1 C). This finding shows that biomass can be considered as a cheap, abundant, and environmentally friendly carbon source for the formation of coating layers on the electrode materials. Therefore, following this trend, this publication describes the preparation of a biomass-derived carbon-coated LTO material and its application as an anode for LIBs. The carbon precursor for coating was obtained from a commercial carrot juice through microwave degradation and was deposited on the LTO material prepared with a well-known sol-gel method. Moreover, the carbon deposition on the LTO was carried out without post-synthesis annealing at high temperatures in an inert or reducing atmosphere, which greatly decreases the time and cost of material manufacturing. The carbon-coated electrode exhibited greatly enhanced electrochemical performance even at high charge/discharge rates in comparison with the pristine LTO electrode.

2. Materials and Methods

2.1. Preparation of Biomass-Derived Carbon Precursor

Commercially available carrot juice was chosen as a source of carbon. It was transferred to a glass container and then heated in a microwave oven (Panasonic Model NN-GT231 M, Osaka, Japan) for 20 min at maximum power. The resulting char product was stirred for 1 h at 1000 rpm with a diluted solution of 0.01 M NaOH of pH 7.4, which acted as a passivating agent. After that, the char carbon was separated from the solution by centrifugation. It was also rinsed several times with water and then sonicated and filtered with Whatman filter paper (Little Chalfont, UK). The biomass-derived carbon precursor was stored in ethanol at room temperature.

2.2. Preparation of Pristine and Carbon-Coated LTO Materials

Pristine LTO material was synthetized through a sol-gel method. In the process, 10.5 g of lithium acetate dihydrate [CH$_3$COOLi·2H$_2$O] (98%, Acros, NJ, USA) and 42.5 g of tetrabutyl titanate [Ti(OC$_4$H$_9$)$_4$] (99%, Acros) were separately dissolved in ethanol (95%, Shimakyu, Samut Sakhon, Thailand). After that, the CH$_3$COOLi·2H$_2$O solution was titrated to the Ti(OC$_4$H$_9$)$_4$ solution. The solutions were continuously stirred at room temperature during the titration until a homogeneous mixture was achieved. Subsequently, ethanol

solution containing a citric acid (99.5%, Acros), which acted as a chelating agent, was poured into the previously obtained solution. The resulting sol-gel precursor solution was composed of $CH_3COOLi:Ti(OC_4H_9)_4$:citric acid at a molar ratio of 4:5:1.25. It was stirred at room temperature for 30 min and then heated at 80 °C for 6 h to obtain a gel precursor, which was further dried at 60 °C for 8 h to remove the remaining solvent. Afterwards, it was preheated at 350 °C for 4 h and cooled to room temperature; then, it was thermally treated with a heating rate of 10 °C min^{-1} up to 800 °C. The gel was left at 800 °C for 12 h under air atmosphere to obtain the pristine LTO material.

The pristine LTO material was used to obtain the biomass-derived carbon-coated LTO labeled as LTO/C. In general, the as-synthesized LTO powder was dispersed in ethanol solution containing the previously prepared biomass-derived carbon precursor. The solution was sonicated for 20 min. After that, it was dried at 60 °C for 8 h to evaporate the ethanol and obtain the dry LTO/C material.

2.3. Characterization of Materials

The morphological properties and particle size of the LTO and LTO/C materials were determined with a scanning electron microscope (SEM; JSM-7800F, JEOL, Akishima, Japan) and a high-resolution transmission electron microscope (HR-TEM; Philips Tecnai G2, Eindhoven, The Netherlands). The structural properties of both LTO samples were analyzed using an X-ray diffractometer (XRD; 6000 Shimadzu Corporation, Kyoto, Japan) operating at 40 kV and 30 mA and equipped with a Cu K$_\alpha$ lamp (λ_{XRD} = 1.5406 Å), a UV-VIS spectrometer (Agilent 8453, Santa Clara, CA, USA) with ethanol as the reference, a Fourier transform infrared spectrometer (FTIR, JASCO FT/IR 6700, Tokyo, Japan), and a Raman spectrometer (iHR550, Horiba, λ_{RS} = 532 nm, Kyoto, Japan). The surface chemical composition of samples was characterized using X-ray photoelectron spectroscopy (XPS, VG ESCA Scientific Theta Probe, Chanhassen, MN, USA). The content of carbon in the LTO/C was estimated by a thermogravimetric analyzer (TGA, Pyris 1, PerkinElmer, Waltham, MA, USA). The TGA measurement was carried out from room temperature to 700 °C with a heating rate of 10 °C min^{-1} in air atmosphere. The specific surface areas and pore sizes of the investigated LTO materials were determined with nitrogen adsorption–desorption measurements performed with an ASAP 2020-Micromeritics analyzer.

2.4. Characterization of Materials

The pristine and carbon-coated LTO materials as active electrode materials, acetylene black (UBIQ Technology Co., San Francisco, CA, USA) as a conductive material, and polyvinylidene fluoride (PVDF) (Kynar HSV 900, Avon Lake, OH, USA) as a binder were mixed at a weight ratio of 83:10:7, were dissolved in N-methyl-2-pyrrolidone (NMP, 99%, Alfa Aesar, Haverhill, MA, USA), and then stirred for 2 h. The obtained slurry was deposited on a current collector, in this work, a copper foil (UBIQ Technology Co.). After that, the current collector with electrode was dried at 120 °C for 12 h in vacuum in order to evaporate the residual solvent.

The electrochemical cells composed of the investigated electrodes, lithium metal, and separator soaked with the 1.0 M LiPF$_6$ in ethylene carbonate (EC):diethyl carbonate (DEC) (1:1, *v/v*) electrolyte (Formosa Plastics Corporation Co., Kaohsiung, Taiwan) were assembled in an argon-filled glove box. The electrochemical tests were prepared using a CR2032 coin-type cell.

The galvanostatic charge and discharge (GCD) and rate capability analyses were performed by a commercial battery auto test system (NEWARE CT-4000, Shenzhen, China) at a potential window between 1.0 and 2.5 V (vs. Li$^+$/Li) at varied current densities at room temperature. The cyclic voltammetry (CV) experiments were collated at a voltage of 1.0–2.5 V (vs. Li$^+$/Li) at various rates with VMP-300 (BioLogic, Seyssinet-Pariset, France). The electrochemical impedance spectroscopy (EIS) analysis was carried out by using a Zahner Zennium (Kronach–Gundelsdorf, Germany) in the frequency range from 0.1 mHz

to 100 kHz with an amplitude of 5 mV. The EIS spectra were collected at a constant potential of 1.587 V.

3. Results and Discussion

The structural properties of the LTO and LTO/C samples were initially analyzed using the XRD technique. The obtained results are shown in Figure 1a. The XRD patterns of both samples were almost the same, indicating that the crystal structure of the pristine LTO material was not influenced by the deposition of the carbon coating. The positions of the peaks matched well to the structure of cubic spinel $Li_4Ti_5O_{12}$ with an Fd3m space group (JCPDS card no. 49-0207). The calculated unit-cell parameter of the LTO/C (a~8.3535 Å) was in line with the unit-cell parameter of the pristine LTO (a~8.35053 Å). No signal related to impurities such as rutile and anatase, which usually exist in LTO materials prepared by sol-gel reactions, was found in the XRD patterns. It is also worth noting that no evidence of carbon was observed for the LTO/C sample. This means that the deposited carbon was amorphous or its content was too low to detect with the XRD technique. Hence, the presence of carbon in the LTO/C was additionally verified by the performance of UV, FTIR, Raman spectroscopy, and XPS investigations.
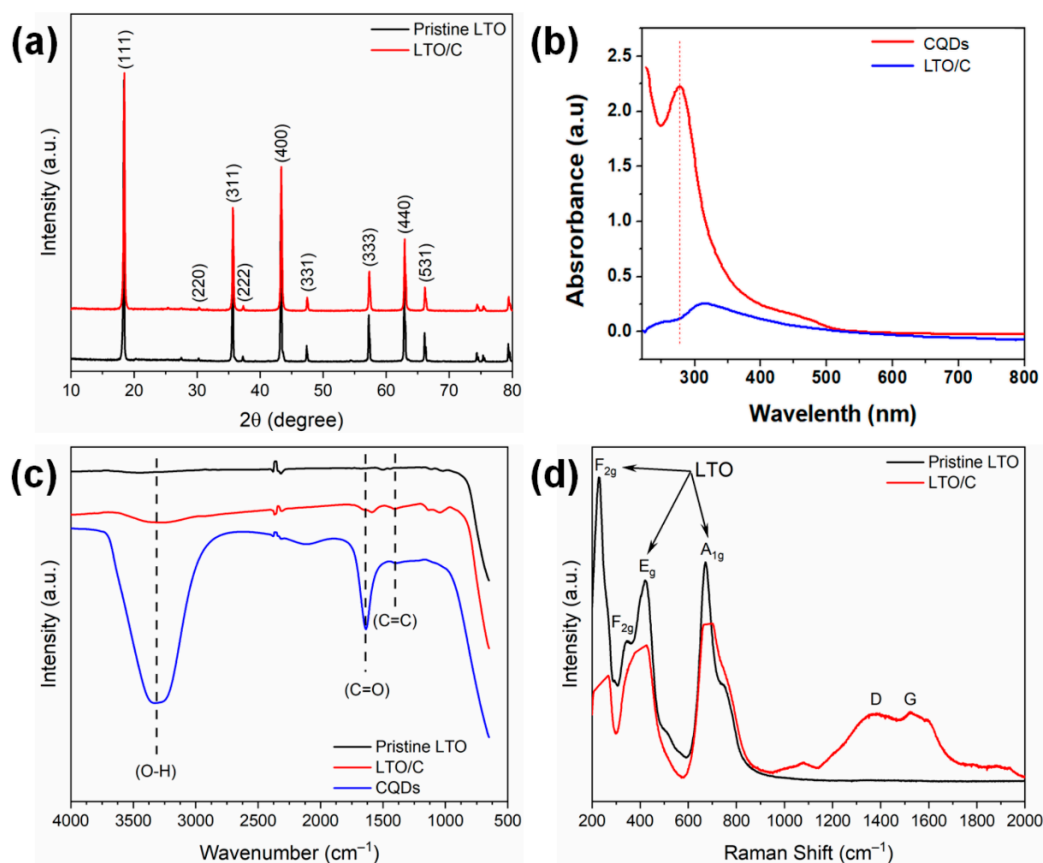
Figure 1. (**a**) XRD patterns of pristine and biomass-derived carbon-coated LTO materials; (**b**) UV-VIS spectra of carbon quantum dots (CQDs) and biomass-derived CQD-coated LTO material; (**c**) FTIR spectra of CQDs, pristine and biomass-derived CQD-coated LTO materials; (**d**) Raman spectra of pristine and biomass-derived CQD-coated LTO materials.

The UV-VIS spectra of carbon precursor and LTO/C dispersed in ethanol are presented in Figure 1b. The spectrum recorded for the carbon precursor reveals a broad and strong absorption peak at 260–320 nm. In fact, this peak is characteristic for carbon quantum dots (CQDs) and typically corresponds to π-π* and n-π* transitions of C=C and C–O bonds [28,29]. In turn, two broad overlapping peaks were visible for the LTO/C sample. The maxima of the first peak matches well to the position of the absorption peak

observed for the carbon precursor, whereas the second peak was associated with the LTO material [30–32]. It is also worth noting that no absorption edge at approximately 435 nm, corresponding to the second-phase Li_2TiO_3, was observed [32]. This is in good agreement with the XRD results and confirmed that the LTO material was quite pure.

The FTIR results are presented in Figure 1c. The spectrum of the biomass-derived CQDs revealed three bands whose maxima were 3315, 1640, and 1400 cm^{-1} corresponding to O–H, C=O, and C=C vibrational modes, respectively [28,29]. The peak associated with O–H came from adsorbed water, whereas the two latter peaks were related to carbon material. All these three peaks were not visible in the spectrum of pristine LTO, but were distinguishable for the LTO/C sample. Their intensities were much lower, which means that the amount of carbon deposited on the LTO was not high.

The Raman spectra shown in Figure 1d revealed five characteristic bands associated with the LTO structure. The band located at 235 cm^{-1} correlated with the bending vibration of the O–Ti–O. The bands at 348 cm^{-1} and 427 cm^{-1} corresponded to the stretching–bending vibrations of the Li–O bonds in LiO_4 and LiO_6 polyhedrons. The last two bands at 679 cm^{-1} and 750 cm^{-1} resulted from the vibrations of Ti–O bonds in TiO_6 octahedra [33–35]. All these bands were very sharp and well defined in the case of LTO material. In turn, they were much lower and somewhat suppressed for the LTO/C sample. Moreover, the three additional bands located at 1100, 1357, and 1592 cm^{-1} appeared in the spectrum of carbon-coated LTO. The origin of the peak at 1100 cm^{-1} is associated with the disordered sp^3 carbon [36,37]. In turn, the peaks at 1357 and 1592 cm^{-1} referred to the D and G bands, respectively, and they are typically observed for graphitic carbon [34,35,38]. Nevertheless, they were very broad and partially overlapping, which suggests that the carbon coating was amorphous [39].

The successful deposition of the carbon coating on the LTO was also confirmed by XPS investigations. The C 1s XPS spectra recorded for the biomass-derived CQDs and the LTO/C material are shown in Figure 2. In fact, they were different. The spectrum of the biomass-derived CQDs was deconvoluted into four bands located at 283.5, 284.4, 286.6, and 291.5 eV corresponding to C–C, C=C, C–O/C=O, and π-π* bonds, respectively [40–44]. In turn, the C 1s XPS spectrum of the LTO/C material was split into four bands located at 281.5, 282.9, 284.4, and 286.5 eV associated with Ti–C, C–C, C=C, and C–O/C=O bonds [38,40–44]. The XPS data were in good agreement with the previously discussed UV-VIS measurements in which the characteristic π-π* transition was observed for the CQDs, whereas this signal was greatly weaker for the LTO/C material.
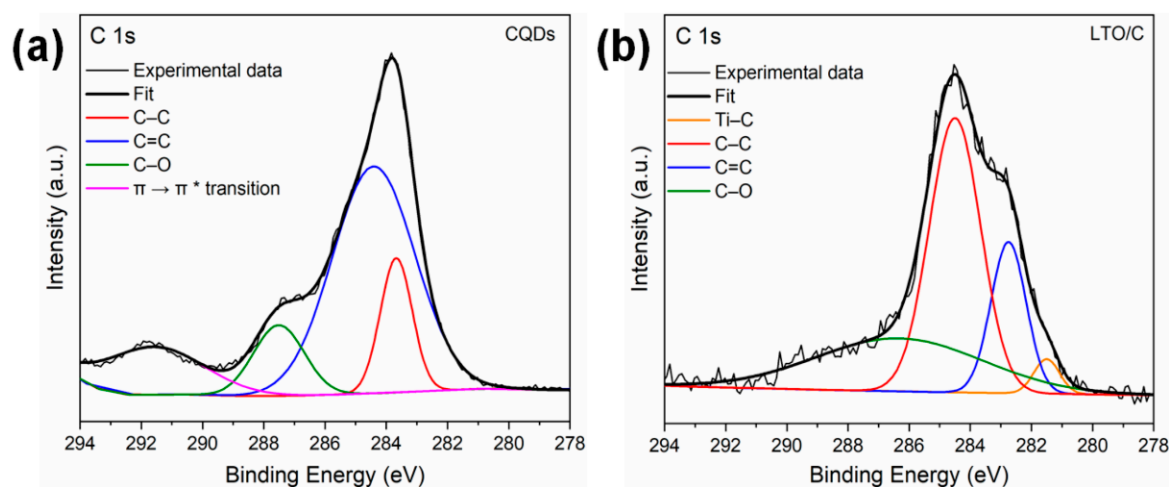
Figure 2. C 1s XPS spectra of (**a**) carbon quantum dots (CQDs) and (**b**) biomass-derived CQD-coated LTO materials.

The thermogravimetric curves recorded for the LTO and LTO/C samples are shown in Figure 3. In fact, they were collected in order to estimate the content of carbon in the LTO/C

material. The TGA curve for the pristine LTO material did not significantly change up to 700 °C. Only one very small mass loss was observed in the temperature range between 250 to 400 °C and this could correspond to the decomposition of some impurities undetectable by XRD, FTIR, and Raman spectroscopy. In turn, the TGA curve for the LTO/C material revealed the first mass drop of about 0.4% up to 100 °C. This corresponded to a release of adsorbed water molecules, which were also detected with the FTIR method. The second mass loss started at about 200 °C and finished at 450 °C. This mass change (~2.6% in relation to the initial mass) was related to a combustion reaction of the carbon coating with oxygen coming from the experimental atmosphere.
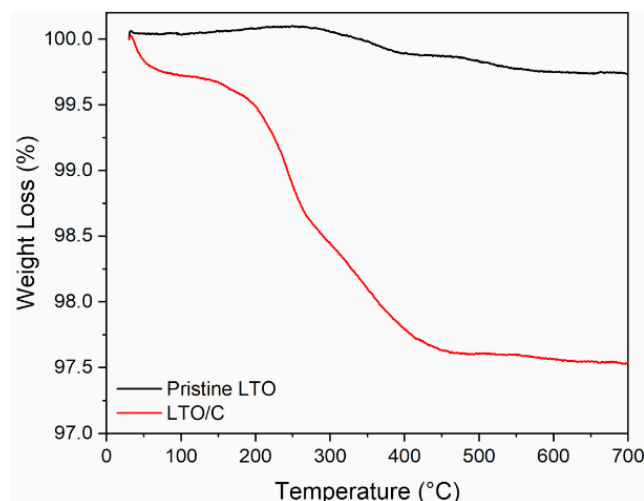

Figure 3. TGA curves recorded for pristine and biomass-derived CDQs-coated LTO materials.

The morphologies and particle sizes of LTO and LTO/C materials were determined with SEM. The collected data is presented in Figure 4. According to the SEM images, the size of the pristine LTO particles was larger than that of LTO/C. The estimated average sizes equaled about 245 and 202 nm for LTO and LTO/C, respectively. Besides that, the particle size distribution of the LTO/C sample was more homogeneous and the surfaces were rougher due to the deposition of carbon coating. The HR-TEM results confirmed this observation (cf. Figure 5a), but they also showed that some of the grain edges exhibited a flat continuous thin coating (cf. Figure 5b). The thickness of both types of observed carbon coatings did not exceed 3 nm. The well adherent carbon cover of the LTO material can constitute a good conductive network for electrons passing through the insulating LTO surface. This, in turn, could be beneficial to enhance the electronic conductivity of the LTO/C material, as well as provide a shorter diffusion pathway for the lithium ions from the electrolyte, resulting in superior rate performance and cycling stability.
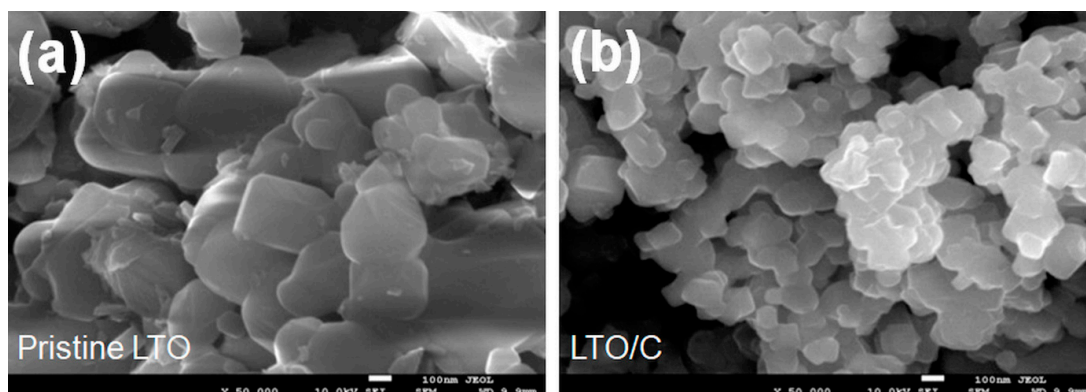

Figure 4. SEM images of (**a**) pristine LTO and (**b**) LTO/C materials.
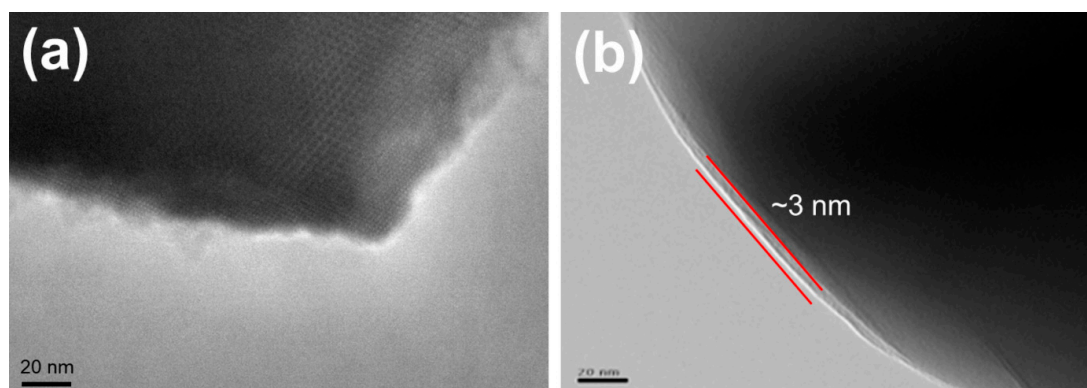
Figure 5. HR-TEM images of (**a**) rough surface and (**b**) flat coating of LTO/C material.

The results coming from the nitrogen adsorption–desorption measurements are shown in Figure 6. The collected isotherms exhibited type IV isotherms with an H1-type hysteresis loop, indicating a mesoporous nature. The values of pore size and specific surface area were estimated using Barret–Joyner–Halenda (BJH) [45] and Brunauer–Emmett–Teller (BET) [46] models, respectively. According to BJH model, the average pore size was 58.7 and 37.7 nm for the pristine and carbon-coated LTO materials, respectively. The specific surface area calculated based on the BET model was 1.434 and 2.076 $m^2 \ g^{-1}$ for the pristine and carbon-coated LTO materials, respectively. The obtained results are in good agreement with the electron microscopy observations. Namely, the larger specific surface area and smaller size of pores found for the LTO/C sample resulted from the roughness and partial filling of the pores caused by the carbon deposition. It is important that the reduction of particle size usually provides access to higher surface area. This, in turn, is beneficial for the high Li-ion flux across electrolyte/electrode interface.
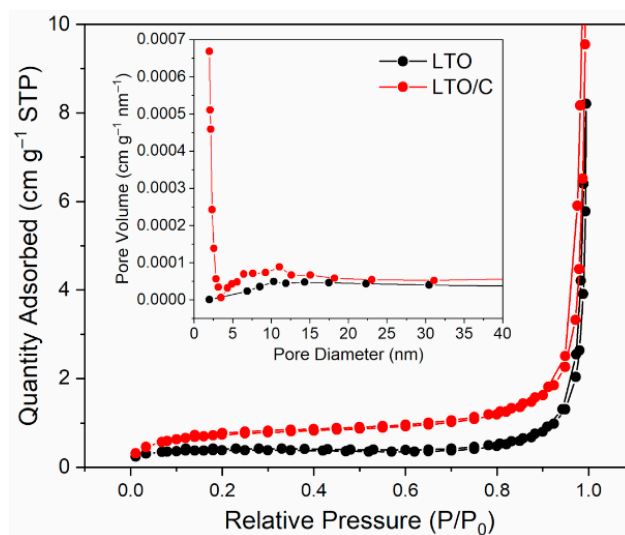
Figure 6. Nitrogen adsorption and desorption isotherms of pristine LTO and LTO/C materials; inset shows the BJH pore-size distributions for both LTO materials.

Cyclic voltammetry (CV) curves for the electrochemical cells with LTO and LTO/C anode materials are in Figure 7. They were recorded with scan rates of 100, 300, and 500 mV s^{-1} at a potential window from 1.0 to 2.5 V (vs. Li^+/Li). The voltammograms for both LTO electrodes revealed only one pair of redox peaks, which corresponded to oxidation and reduction processes of the Ti^{3+}/Ti^{4+} couple [25,27,35]. No other redox peaks were observed, which indicates that the carbon coating did not alter the electrochemical reaction process in the given potential range. Nevertheless, the peaks obtained for the LTO/C electrode were much sharper than those of the pristine LTO anode. This can be

explained by the faster Li$^+$ ion insertion/extraction in the case of the LTO/C electrode [47]. In addition, the carbon-coated LTO electrode showed a smaller potential difference ΔE between two redox peaks than the pristine LTO for all scan rates. This suggests that the carbon coating could efficiently diminish polarization behavior, as well as enhance the rate capability of the LTO/C electrode.
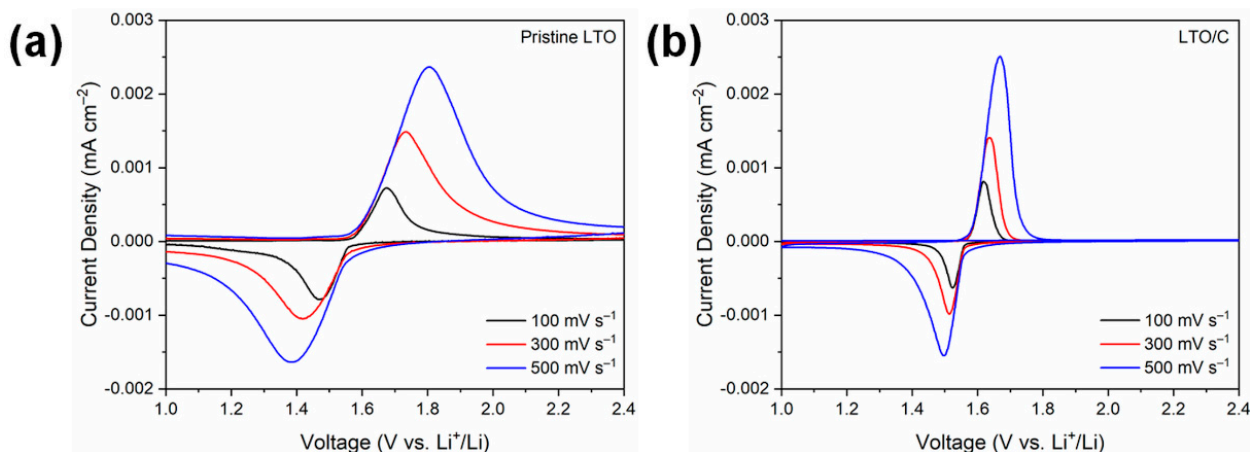
Figure 7. CV curves recorded with scan different rates for (**a**) pristine LTO and (**b**) LTO/C electrodes.

The EIS data recorded for LTO and LTO/C electrodes and their corresponding equivalent circuit models are shown in Figure 8. The shapes of the EIS spectra were similar and were composed of a semicircle at high frequency and one slope line at low frequency. An intercept at high frequency corresponded to the ohmic resistance (R_s) between the electrolyte and electrode. The large semicircle at high frequency was associated with the charge transfer resistance (R_{ct}) and the constant phase element (CPE) corresponding to double layer capacitance at the electrode/electrolyte interface. The inclined line at low frequency was related to the Warburg impedance (W), which referred to a solid state diffusion of Li$^+$ ions into the LTO structure. The fitted R_{ct} for the LTO and LTO/C electrodes was 40.81 and 19.37 Ω, respectively. The lower value found for the LTO/C material was associated with the carbon coating. which facilitated the electrochemical kinetics of the Ti^{3+} and Ti^{4+} redox reaction by the increase of the surface electrical conductivity. The presence of a carbon layer reduced the electrode polarization of the LTO, which agreed with the CV investigations. Furthermore, the Li-ion diffusion coefficient was determined for the pristine and carbon-coated LTO electrodes based on the equations:

$$D_{\mathrm{Li}} = \frac{R^2 T^2}{2A^2 n^4 \mathrm{F}^4 C^2 \sigma^2}, \tag{1}$$

$$Z' = R_s + R_{ct} + \sigma \omega^{-0.5}, \tag{2}$$

where D_{Li} is the Li$^+$ diffusion coefficient, R is the gas constant (8.314 J mol^{-1} K^{-1}), T is the room temperature (298 K), A is the surface area of the electrode (0.785 cm^2), n is the number of electrons during the half reaction of the redox couple (equal to 1), F is the Faraday constant (96,500 C mol^{-1}), C is the molar concentration of Li$^+$ ions, σ is the Warburg impedance coefficient, and ω is the angular frequency in the low-frequency region. The σ was delivered from the relationship between the real axis of resistance (Z$'$) and the reciprocal square root of the frequency ($\omega^{-0.5}$) in the low-frequency region shown in Figure 8b. The performed calculations allowed estimating the diffusion coefficient, which equaled 3.4×10^{-12} and 1.0×10^{-11} cm^2 s^{-1} for the pristine LTO and LTO/C electrodes, respectively. The obtained values confirmed that the carbon coating provided the shorter diffusion pathways for the Li$^+$ ion into the LTO structure.
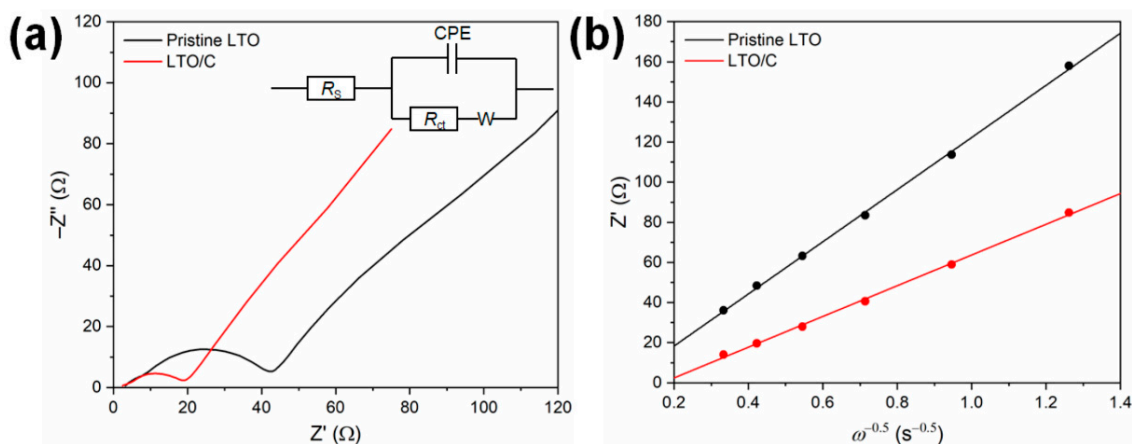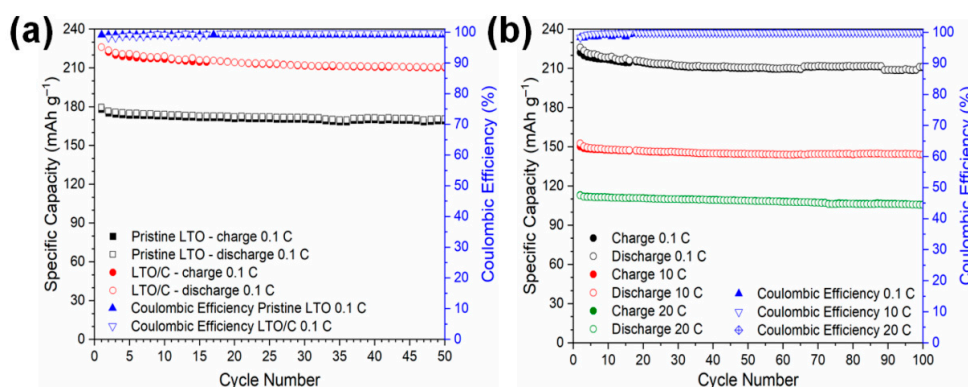
Figure 8. (**a**) EIS plots of pristine LTO and LTO/C electrodes (inset shows the equivalent circuit model used to fit the obtained EIS spectra); (**b**) graph of Z' against $\omega^{-0.5}$ at the low frequency region.

The electrochemical performance of the investigated LTO materials as anodes for LIBs was evaluated via room temperature galvanostatic discharge/charge tests. The initial charge–discharge profiles of LTO and LTO/C electrodes recorded with 0.1 C, 2 C, 5 C, 10 C, and 20 C rates (1 C = 175 mA g^{-1}) are shown in Figure 9. Analyzing them, one can see that the flat discharge and charges plateaus at approximately 1.5 and 1.6 V, respectively, were well defined. They were associated with the reversible Ti^{3+}/Ti^{4+} redox reactions corresponding to the insertion/extraction of Li$^+$ ions into the spinel structure. It is also worth noting that additional plateaus for charge and discharge profiles appeared for the LTO/C electrodes cycled at high C-rates above 2 C. Their origin was associated with the pseudocapacitive effect induced by the presence of the carbon coating [47–50]. Thus far, it has been reported that this pseudocapacitive behavior improves the capacity and high-rate capability [47]. This is in good agreement with the obtained results for the LTO/C electrode investigated in this work. It is important that an interval of the middle sections of the charge and discharge plateaus observed for the LTO/C sample was distinctly lower than that of the pristine LTO electrode. This observation was related to lower electrode polarization. The initial discharge capacity recorded for LTO and LTO/C electrodes at 0.1 C was about 177 and 213 mAh g^{-1}, respectively. Undoubtedly, the lower polarization and the higher capacity observed for LTO/C sample resulted from the presence of carbon, which shortened the Li$^+$ diffusion pathways and enhanced the electronic conductivity of LTO material. Moreover, the carbon-coated LTO electrode had the higher surface area, which offered more active sites for the storage of Li$^+$ ions. It was also evident that the increase of cycling rate up to 10 C and 20 C caused a more significant drop of initial capacity for the pristine LTO.
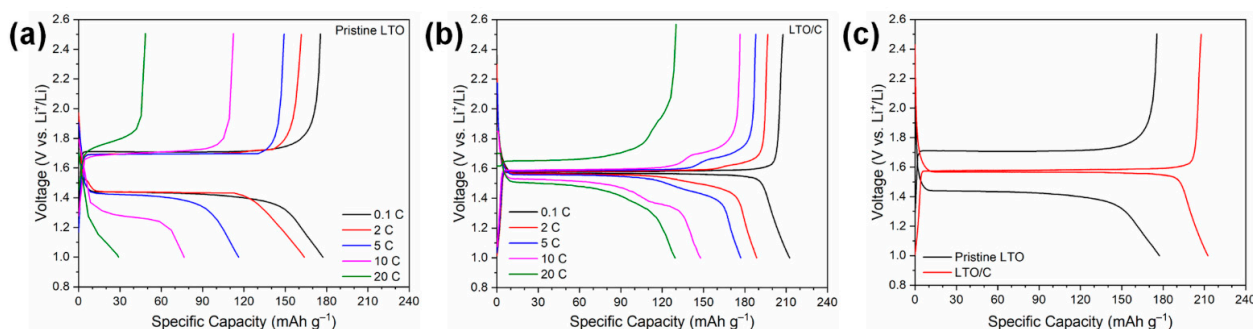

Figure 9. Room temperature initial charge/discharge profiles recorded for (**a**) pristine LTO and (**b**) LTO/C electrodes at different current rates between 1.0 and 2.5 V vs. Li$^+$/Li; (**c**) comparison of initial profiles of pristine LTO and LTO/C electrodes recorded at 0.1 C rate.

The cycling performance tests of LTO and LTO/C electrodes are shown in Figure 10. The obtained results indicate that both investigated materials had stable cycling life during 50 consecutive discharge–charge cycles. The Coulombic efficiency was established at the level of approximately 100%, indicating that the electrochemical Li$^+$ lithiation–delithiation processes are entirely reversible. However, it should be noted that the LTO/C electrode exhibited significantly higher capacity of about 211 mAh g^{-1} after 50 cycles, whereas the capacity of the LTO was around 171 mAh g^{-1}. The capacity for LTO/C did not change even after 100 cycles at 0.1 C. In turn, the increase of charge–discharge rate up to 10 C and 20 C caused a drop of capacity equal to 144 and 106 mAh g^{-1} after 100 cycles, respectively. The performed tests indicated that the cycling performance of the LTO/C electrode was very stable during the cycling, even at high rates.

Figure 10. (**a**) Cycling performance and coulombic efficiency of pristine LTO and LTO/C electrodes at 0.1 C rate; (**b**) long term cycling performance and coulombic efficiency of LTO/C measured at 0.1 C and 10 C.

To investigate the effect of carbon coating on electrochemical performance, the rate capabilities of LTO, and LTO/C electrodes were tested at different current densities from 0.1 to 20 C, as shown in Figure 11. According to the obtained results, the LTO/C electrode exhibited better cycling response to continuously varied current densities than the pristine LTO electrode. This observation was based on the specific capacity for the LTO significantly decreasing with the increasing C-rate. The LTO and LTO/C electrodes achieved capacities of 173 and 203 mAh g^{-1}, respectively, at the initial 0.1 C rate. As the current rate increased from 0.1 to 2, 5, 10, and 20 C, the capacity decreased to 152 (88% retention), 112 (65% retention), 74 (43% retention), and 27 (16% retention) mAh g^{-1} for the LTO electrode and 191 (94% retention), 153 (75% retention), 135 (67% retention), and 107 (53% retention) mAh g^{-1} for the LTO/C electrode. In turn, when the current rate came back to 0.1 C, the capacities returned to their initial values. This indicates that the capacity fade for the LTO/C was reduced by the presence of carbon coating. which provided (i) shorter distance for solid-state diffusion of the Li$^+$ ions during the charge and discharge cycling, and (ii) higher surface area and conductivity, confirmed by BET and EIS measurements, respectively.
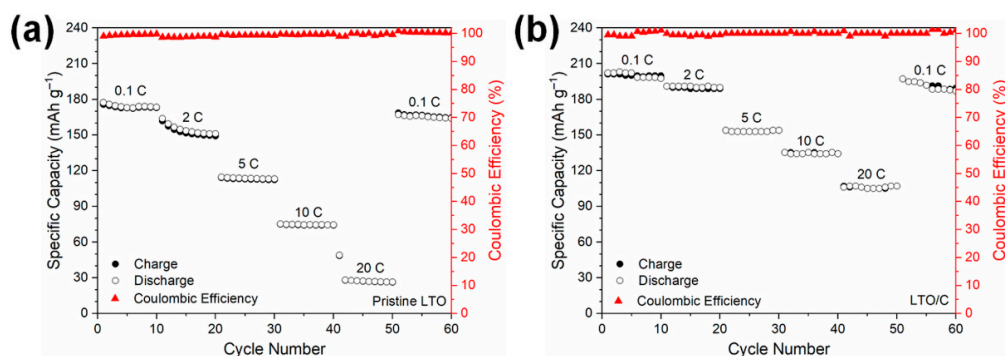
Figure 11. Rate capability and coulombic efficiency of (**a**) pristine LTO and (**b**) LTO/C electrodes.

4. Conclusions

This work presents the successful preparation of carbon-coated LTO material and its application as the anode material for the Li-ion batteries. The pristine LTO material was synthetized through the sol-gel process and then was covered with a thin carbon coating obtained from carrot juice. The LTO/C electrode revealed enhanced conductivity, cyclic stability, and excellent high-rate capability in comparison with the pristine LTO electrode. The LTO/C exhibited a high reversible specific capacity of 212 mAh g^{-1} at 0.1 C at the potential window between 1.0 and 2.5 V, even after 100 cycles. Moreover, the capacity retention reached 53% of the initial value when the charge–discharge rate increased from 0.1 C to 20 C. Its excellent electrochemical performance was attributed to the presence of carbon coating, which provided (i) shorter diffusion pathways for the Li$^+$ ions into the LTO structure during the charge and discharge cycling, and (ii) higher surface area and conductivity, confirmed by BET as well as EIS measurements, respectively. The obtained results indicate that the investigated LTO/C electrode fulfils the necessary requirements to be the anode material for the future high-rate lithium-ion batteries.

Data Availability Statement: Not applicable.

Conflicts of Interest: The authors declare no conflict of interest.

References

1. Liu, Y.Y.; Zhou, G.M.; Liu, K.; Cui, Y. Design of complex nanomaterials for energy storage: Past success and future opportunity. *Acc. Chem. Res.* **2017**, *50*, 2895–2905. [CrossRef]
2. Asenbauer, J.; Eisenmann, T.; Kuenzel, M.; Kazzazi, A.; Chen, Z.; Bresser, D. The success story of graphite as a lithium-ion anode material—Fundamentals, remaining challenges, and recent developments including silicon (oxide) composites. *Sustain. Energy Fuels* **2020**, *4*, 5387–5416. [CrossRef]
3. Wu, J.X.; Cao, Y.L.; Zhao, H.M.; Mao, J.F.; Guo, Z.P. The critical role of carbon in marrying silicon and graphite anodes for high-energy lithium-ion batteries. *Carbon Energy* **2019**, *1*, 57–76. [CrossRef]
4. Seo, J.H.; Verlinde, K.; Rajagopalan, R.; Gomez, E.D.; Mallouk, T.E.; Randall, C.A. Cold sintering process for fabrication of a high volumetric capacity Li$_4$Ti$_5$O$_{12}$ anode. *Mater. Sci. Eng. B* **2019**, *250*, 114435. [CrossRef]
5. Iniguez, F.B.; Jeong, H.; Mohamed, A.Y.; Nogales, P.M.; Choi, H.; Jeong, S.K.; Park, J.B.; Kim, Y.S.; Cho, D.Y. Structure and electrochemical properties of CNT-supported Li-Ti-O anode material for Li-ion battery. *J. Ind. Eng. Chem.* **2022**, *112*, 125–133. [CrossRef]
6. Yi, T.F.; Yang, S.Y.; Xie, Y. Recent advances of Li$_4$Ti$_5$O$_{12}$ as a promising next generation anode material for high power lithium-ion batteries. *J. Mater. Chem. A* **2015**, *3*, 5750–5777. [CrossRef]
7. Pang, S.P.; Zhao, Y.Y.; Zhang, C.J.; Zhang, Q.H.; Gu, L.; Zhou, X.H.; Li, G.C.; Cui, G.L. Electrostatic assembly of mesoporous Li$_4$Ti$_5$O$_{12}$/graphene hybrid as high-rate anode materials. *Scr. Mater.* **2013**, *69*, 171–174. [CrossRef]
8. Wang, J.; Liu, X.M.; Yang, H.; Shen, X.D. Characterization and electrochemical properties of carbon-coated Li$_4$Ti$_5$O$_{12}$ prepared by a citric acid sol–gel method. *J. Alloys Compd.* **2011**, *509*, 712–718. [CrossRef]
9. Li, J.R.; Tang, Z.L.; Zhang, Z.T. Controllable formation and electrochemical properties of one-dimensional nanostructured spinel Li$_4$Ti$_5$O$_{12}$. *Electrochem. Commun.* **2005**, *7*, 894–899. [CrossRef]
10. Prakash, A.S.; Manikandan, P.; Ramesha, K.; Sathiya, M.; Tarascon, J.M.; Shukla, A.K. Solution-combustion synthesized nanocrystalline Li$_4$Ti$_5$O$_{12}$ as high-rate performance Li-ion battery anode. *Chem. Mat.* **2010**, *22*, 2857–2863. [CrossRef]
11. Li, K.M.; Dai, X.D.; Manawan, M.; Wang, Q.; Pan, J.H. Unveiling the formation mechanism and phase purity control of nanostructured Li$_4$Ti$_5$O$_{12}$ via a hydrothermal process. *Cryst. Growth Des.* **2021**, *21*, 5440–5450. [CrossRef]
12. Du, G.D.; Sharma, N.; Peterson, V.K.; Kimpton, J.A.; Jia, D.Z.; Guo, Z.P. Br-doped Li$_4$Ti$_5$O$_{12}$ and composite TiO$_2$ anodes for Li-ion batteries: Synchrotron X-ray and in situ neutron diffraction studies. *Adv. Funct. Mater.* **2011**, *21*, 3990–3997. [CrossRef]
13. Ma, Y.; Ding, B.; Ji, G.; Lee, J.Y. Carbon-encapsulated F-doped Li$_4$Ti$_5$O$_{12}$ as a high rate anode material for Li$^+$ batteries. *ACS Nano* **2013**, *7*, 10870–10878. [CrossRef]

14. Lin, C.F.; Lai, M.O.; Lu, L.; Zhou, H.H.; Xin, Y.L. Structure and high rate performance of Ni^{2+} doped $Li_4Ti_5O_{12}$ for lithium ion battery. *J. Power Sources* **2013**, *244*, 272–279. [CrossRef]

15. Xue, X.X.; Yan, H.Y.; Fu, Y.Q. Preparation of pure and metal-doped $Li_4Ti_5O_{12}$ composites and their lithium-storage performances for lithium-ion batteries. *Solid State Ion.* **2019**, *335*, 1–6. [CrossRef]

16. Liu, Z.F.; Cao, L.; He, F.L.; Zhang, Z.W.; Li, D.; Zhao, W.; Qi, T. Study on the possibility of diagonal line rule in elemental doping effects in $Li_4Ti_5O_{12}$ by mechanochemical method. *Electrochim. Acta* **2022**, *422*, 140485. [CrossRef]

17. Kang, C.Y.; Krajewski, M.; Lin, J.Y. Impact of titanium precursors on formation and electrochemical properties of $Li_4Ti_5O_{12}$ anode materials for lithium-ion batteries. *J. Solid State Electrochem.* **2021**, *25*, 575–582. [CrossRef]

18. Wang, Y.G.; Liu, H.M.; Wang, K.X.; Eiji, H.; Wang, Y.R.; Zhou, H.S. Synthesis and electrochemical performance of nano-sized $Li_4Ti_5O_{12}$ with double surface modification of Ti(III) and carbon. *J. Mater. Chem.* **2009**, *19*, 6789–6795. [CrossRef]

19. Jung, H.G.; Myung, S.T.; Yoon, C.S.; Son, S.B.; Oh, K.H.; Amine, K.; Scrosati, B.; Sun, Y.K. Microscale spherical carbon-coated $Li_4Ti_5O_{12}$ as ultra high power anode material for lithium batteries. *Energy Environ. Sci.* **2011**, *4*, 1345–1351. [CrossRef]

20. Zhu, Z.Q.; Cheng, F.Y.; Chen, J. Investigation of effects of carbon coating on the electrochemical performance of $Li_4Ti_5O_{12}$/C nanocomposites. *J. Mater. Chem. A* **2013**, *1*, 9484–9490. [CrossRef]

21. Li, Z.Y.; Ding, F.X.; Zhao, Y.G.; Wang, Y.D.; Li, J.L.; Yang, K.; Gao, F. Synthesis and electrochemical performance of $Li_4Ti_5O_{12}$ submicrospheres coated with TiN as anode materials for lithium-ion battery. *Ceram. Int.* **2016**, *42*, 15464–15470. [CrossRef]

22. Jin, Y.; Yu, H.; Gao, Y.; He, X.Q.; White, T.A.; Liang, X.H. $Li_4Ti_5O_{12}$ coated with ultrathin aluminum-doped zinc oxide films as an anode material for lithium-ion batteries. *J. Power Sources* **2019**, *436*, 226859. [CrossRef]

23. Lv, S.X.; Chen, Q.L.; Song, F.X.; Li, Y.N. One-step synthesis of a double conductive layer $C-SiO_x-TiO_2$ co-coated $Li_4Ti_5O_{12}$ anode material toward a high-rate and large-capacity lithium-ion battery. *Appl. Surf. Sci.* **2021**, *555*, 149637. [CrossRef]

24. Zhao, Y.Y.; Pang, S.P.; Zhang, C.J.; Zhang, Q.H.; Gu, L.; Zhou, X.H.; Li, G.C.; Cui, G.L. Nitridated mesoporous $Li_4Ti_5O_{12}$ spheres for high-rate lithium-ion batteries anode material. *J. Solid State Electrochem.* **2013**, *17*, 1479–1485. [CrossRef]

25. Dhaiveegan, P.; Peng, H.T.; Michalska, M.; Xiao, Y.M.; Lin, J.Y.; Hsieh, C.K. Investigation of carbon coating approach on electrochemical performance of $Li_4Ti_5O_{12}$/C composite anodes for high-rate lithium-ion batteries. *J. Solid State Electrochem.* **2018**, *22*, 1851–1861. [CrossRef]

26. Hsu, S.C.; Huang, T.T.; Wu, Y.J.; Lu, C.Z.; Weng, H.C.; Huang, J.H.; Chang-Jian, C.W.; Liu, T.Y. Polyimide-derived carbon-coated $Li_4Ti_5O_{12}$ as high-rate anode materials for lithium ion batteries. *Polymers* **2021**, *13*, 1672. [CrossRef]

27. Li, K.Q.; Zhang, Y.; Sun, Y.N.; Xu, Y.L.; Zhang, H.; Ye, P.; Zheng, M.D.; Zhou, N.; Wang, D. Template-free synthesis of biomass-derived carbon coated $Li_4Ti_5O_{12}$ microspheres as high performance anodes for lithium-ion batteries. *Appl. Surf. Sci.* **2018**, *459*, 572–582. [CrossRef]

28. Dager, A.; Uchida, T.; Maekawa, T.; Tachibana, M. Synthesis and characterization of monodisperse carbon quantum dots from fennel seeds: Photoluminescence analysis using machine learning. *Sci. Rep.* **2019**, *9*, 14004. [CrossRef]

29. Ghosh, S.; Satapathy, S.S.; Ghosh, K.; Jauhari, S.; Panda, S.K.; Si, S. Carbon dots assisted synthesis of gold nanoparticles and their catalytic activity in 4-nitrophenol reduction. *ChemistrySelect* **2019**, *4*, 3416–3422. [CrossRef]

30. Meng, X.D.; Wang, X.C.; Zhou, Y.X.; Tong, L.; Zeng, X.H.; Chen, X.B. Spinel lithium titanate from brookite nanocrystallites. *Ceram. Int.* **2014**, *40*, 4989–4993. [CrossRef]

31. Jhan, Y.R.; Duh, J.G. Electrochemical performance and low discharge cut-off voltage behavior of ruthenium doped $Li_4Ti_5O_{12}$ with improved energy density. *Electrochim. Acta* **2012**, *63*, 9–15. [CrossRef]

32. Li, Y.A.; Chen, Q.L.; Meng, Q.Q.; Lei, S.L.; Li, C.Q.; Li, X.Y.; Ma, J.B. One-step synthesis of a nanosized cubic Li_2TiO_3-Coated Br, C, and N Co-Doped $Li_4Ti_5O_{12}$ anode material for stable high-rate lithium-ion batteries. *ACS Appl. Mater. Interfaces* **2019**, *11*, 25804–25816. [CrossRef] [PubMed]

33. Li, X.; Lin, H.C.; Cui, W.J.; Xiao, Q.; Zhao, J.B. Fast solution-combustion synthesis of nitrogen-modified $Li_4Ti_5O_{12}$ nanomaterials with improved electrochemical performance. *ACS Appl. Mater. Interfaces* **2014**, *6*, 7895–7901. [CrossRef]

34. Wu, C.Y.; Wang, Y.X.; Xie, J.; Cao, G.S.; Zhu, T.J.; Zhao, X.B. Electrochemical performance of $Li_4Ti_5O_{12}$/carbon nanofibers composite prepared by an in situ route for Li-ion batteries. *J. Solid State Electrochem.* **2012**, *16*, 3915–3921. [CrossRef]

35. Lan, C.K.; Chang, C.C.; Wu, C.Y.; Chen, B.H.; Duh, J.G. Improvement of the Ar/N_2 binary plasma-treated carbon passivation layer deposited on $Li_4Ti_5O_{12}$ electrodes for stable high-rate lithium ion batteries. *RSC Adv.* **2015**, *5*, 92554–92563. [CrossRef]

36. Paillard, V. On the origin of the 1100 cm^{-1} Raman band in amorphous and nanocrystalline sp^3 carbon. *Europhys. Lett.* **2001**, *54*, 194–198. [CrossRef]

37. Korepanov, V.I.; Hamaguchi, H.O.; Osawa, E.; Ermolenkov, V.; Lednev, I.K.; Etzold, B.J.M.; Levinson, O.; Zousman, B.; Epperla, C.P.; Chang, H.C. Carbon structure in nanodiamonds elucidated from Raman spectroscopy. *Carbon* **2017**, *121*, 322–329. [CrossRef]

38. Zhang, L.H.; Koka, R.V. A study on the oxidation and carbon diffusion of TiC in alumina titanium carbide ceramics using XPS and Raman spectroscopy. *Mater. Chem. Phys.* **1998**, *57*, 23–32. [CrossRef]

39. Friederici, L.; Mesceriakove, S.M.; Neumann, A.; Sermyagina, E.; Mescerlakovas, A.; Lahde, A.; Grimmer, C.; Streibel, T.; Ruger, C.P.; Zimmermann, R. Effect of hydrothermal carbonization and eutectic salt mixture (KCl/LiCl) on the pyrolysis of Kraft lignin as revealed by thermal analysis coupled to advanced high-resolution mass spectrometry. *J. Anal. Appl. Pyrolysis* **2022**, *166*, 105604. [CrossRef]

40. Cong, Y.; Li, X.K.; Qin, Y.; Dong, Z.J.; Yuan, G.M.; Cui, Z.W.; Lai, X.J. Carbon-doped TiO_2 coating on multiwalled carbon nanotubes with higher visible light photocatalytic activity. *Appl. Catal. B Environ.* **2011**, *107*, 128–134. [CrossRef]

41. Yun, B.N.; Du, H.L.; Hwang, J.Y.; Jung, H.G.; Sun, Y.K. Improved electrochemical performance of boron-doped carbon-coated lithium titanate as an anode material for sodium-ion batteries. *J. Mater. Chem. A* **2017**, *5*, 2802–2810. [CrossRef]

42. Chaisit, S.; Chanlek, N.; Khajonrit, J.; Sichumsaeng, T.; Maensiri, S. Preparation, characterization, and electrochemical properties of KOH-activated carbon from cassava root. *Mater. Res. Express* **2020**, *7*, 105605. [CrossRef]

43. Park, J.; Back, T.; Mitchel, W.C.; Kim, S.S.; Elhamri, S.; Boeckl, J.; Fairchild, S.B.; Naik, R.; Voevodin, A.A. Approach to multifunctional device platform with epitaxial graphene on transition metal oxide. *Sci. Rep.* **2015**, *5*, 14374. [CrossRef]

44. Zeng, L.; Liu, X.Q.; Chen, X.G.; Soutis, C. π-π interaction between carbon fibre and epoxy resin for interface improvement in composites. *Compos. Part B Eng.* **2021**, *220*, 108983. [CrossRef]

45. Barrett, E.P.; Joyner, L.G.; Halenda, P.P. The determination of pore volume and area distributions in porous substances. I. Computations from nitrogen isotherms. *J. Am. Chem. Soc.* **1951**, *73*, 373–380. [CrossRef]

46. Brunauer, S.; Emmett, P.H.; Teller, E. Adsorption of gases in multimolecular layers. *J. Am. Chem. Soc.* **1938**, *60*, 309–319. [CrossRef]

47. Ding, Y.; Li, G.R.; Xiao, C.W.; Gao, X.P. Insight into effects of graphene in $Li_4Ti_5O_{12}$/carbon composite with high rate capability as anode materials for lithium ion batteries. *Electrochim. Acta* **2013**, *102*, 282–289. [CrossRef]

48. Lai, C.; Dou, Y.Y.; Li, X.; Gao, X.P. Improvement of the high rate capability of hierarchical structured $Li_4Ti_5O_{12}$ induced by the pseudocapacitive effect. *J. Power Sources* **2010**, *195*, 3676–3679. [CrossRef]

49. Li, X.; Lai, C.; Xiao, C.W.; Gao, X.P. Enhanced high rate capability of dual-phase $Li_4Ti_5O_{12}$-TiO_2 induced by pseudocapacitive effect. *Electrochim. Acta* **2011**, *56*, 9152–9158. [CrossRef]

50. Chen, X.; Chen, J.Q.; Zhou, X.Y.; You, M.; Zhang, C.; Yue, W.B. Two-dimensional graphene-based $Li_4Ti_5O_{12}$ with hierarchical pore structure and large pseudocapacitive effect as high-rate and long-cycle anode material for lithium-ion batteries. *Electrochim. Acta* **2022**, *405*, 139814. [CrossRef]